Proceedings of the ASME 2010 3rd Joint US-European Fluids Engineering Summer Meeting and 8th International Conference on Nanochannels, Microchannels, and Minichannels
FEDSM-ICNMM2010
August 1-5, 2010, Montreal, Canada

FEDSM-ICNMM2010-30521

NUMERICAL SIMULATION OF START-UP JETS IN A MIXING CHAMBER

Chenzhou Lian
Purdue University
West Lafayette, IN, USA

Dmytro M. Voytovych
Purdue University
West Lafayette, IN, USA

Guoping Xia
Purdue University
West Lafayette, IN, USA

Charles L. Merkle
Purdue University
West Lafayette, IN, USA

ABSTRACT

Numerical simulations of a transient flow of helium injected into an established background flow of nitrogen were carried out to identify the dominant features of the transient mixing process between these two dissimilar gases. The geometry of interest is composed of two helium slots on either side of a central nitrogen channel feeding into a 'two-dimensional' mixing chamber. Simulations were accomplished on both two- and three-dimensional grids using an unsteady DES approach. Results are compared with experimental measurements of species distributions. Unsteady 2-D solutions give a reasonable qualitative picture of the transient mixing process in the middle of the chamber and enable cost-effective parametric analyses and grid refinement studies. The 2-D solutions also provide quantitative estimates of representative characteristic times to guide the 3-D calculations. The 3-D solutions give a reasonable approximation to span-wise events.

INTRODUCTION

The mixing process between co-flowing jets constitutes a problem of fundamental interest in fluid mechanics that has drawn broad attention from both experimentalists and modelers. Mixing layer studies have included both planar and round jets, discharge into open and confined environments, study of parametric effects such as momentum ratio and density ratio, Reynolds number effects and the effect of boundary layer thickness at the injection plane and details of the geometry of the splitter plate and the exit plane [1-10]. One reason for the broad appeal of this quite fundamental problem is that the configuration appears in various forms in a wide range of applications that arise in diverse engineering systems.

Early mixing studies focused primarily on determining the time-averaged characteristics of mixing layers to deduce features such as the intact core length and their asymptotic rate of spread. Other studies dealt with determining appropriate eddy viscosity models that could be used in RANS analysis to match the velocity profiles in mixing layers. More recently, the primary focus of mixing layer studies has been concerned with the unsteady dynamics of these flows [1, 4, 9, 11, 12] whose time-averaged character is well documented. Similarly recent experiments have focused on documentation of the unsteady character of these mixing problems.

A generic conclusion of this previous work is that mixing is an unsteady problem in which the dynamics of large scale motions contribute greatly to the global process. Most, if not all, of these previous mixing layer studies have, however, addressed the dynamics of statistically stationary jets whose time-averaged flow has been established and whose spatial evolution is being assessed. There appear to be no papers devoted to addressing the characteristics of the manner in which these stationary flows are established. The present paper represents a digression from these previous analyses in that it focuses on the mixing process between jets that are themselves developing in a temporal sense. In particular, we consider the specific problem of the manner in which the dynamics of mixing layers are established during their formative stages.

The experimental background for the present simulations is described in Refs. 13-15. A classical confined, planar mixing layer was established in two steps. In the first step, a single, planar jet of nitrogen was injected into a chamber filled with quiescent gas and the ensuing transient process was followed until all initial perturbations were washed out and the single jet became statistically steady. The second step involved injecting

helium into this established background flowfield of nitrogen from slots parallel to, and on either side of, the nitrogen slot to study the transient mixing between these two gases of dissimilar molecular weight. The chosen mixing sequence is predicated upon the particular application of interest: characterizing the pre-ignition environment in a rocket engine that burns hydrogen and oxygen. The chosen fluids are surrogates for these propellants having similar molecular weight ratios. The geometry is a 'two-dimensional' experimental representation of a representative research device.

The purpose of the present paper is to use both 2-D and 3-D unsteady computations based upon a DES model [16-19] to predict the flowfield inside the chamber. While 2-D simulations can provide parametric study for pertinent phenomena and give guidance for initial 3-D computations. A characteristic feature of the problem is the strong recirculation zones that dominate the dynamics. An intimate understanding of the critical issues in these regions is important before beginning such a computation. The DES simulations are expected to provide a qualitative understanding of the physics of the transient portion of an unsteady problem with significant recirculation zones.

The structure of the paper is as follows. First we describe the geometrical configuration and computational procedures. Then, we present 2-D simulation results and comparisons with the experimental measurements followed by 3-D results and comparisons. Finally, we close the paper with a summary and a perspective of future work.

PROBLEM DEFINITION

The geometry is shown pictorially in Figs. 1 and 2 [15]. Fig. 1 gives an overall view of the rectangular mixing chamber and injector combination while Fig. 2 shows a cross sectional view of the chamber alone. Helium (outer two passages) and nitrogen (central passage) flow through three long, narrow channels before exhausting into the rectangular mixing chamber through three, parallel slots. The mixing chamber is 203.4 *mm* long in the flow direction, 38 *mm* high in the direction perpendicular to the slots and 101.6 *mm* wide in the direction parallel to the slots. The 203.4 *mm* chamber length includes a canted nozzle section that is 25.4 *mm* in length and converges to an exit height of 12.7 *mm* providing a contraction ratio of 3:1 at the exit. This convergent section was incorporated to increase the exhaust velocity at the exit plane and decrease the possibility of inflow over parts of the large rectangular exit area as a result of computational simulations done in conjunction with the experimental design. The Mach number in the throat remained small and the chamber pressure was nominally atmospheric.

The injector that feeds the gases into the mixing chamber is 101.6 *mm* in length and contains three slots extending across the entire 101.6 *mm* span of the chamber. The injector length was chosen to ensure fully developed turbulent flow at the chamber entrance. The central N_2 channel was 3.2 *mm* wide while the two outer He channels were each 1.6 *mm*. The three channels were separated by splitter plates of 1.6 *mm* thickness. The three inlet slots were centered across the chamber width producing a 14.3 *mm* back step between the outer edge of the helium channels and the outer chamber walls. This back step formed a dominant recirculation zone that significantly affected the flow field.

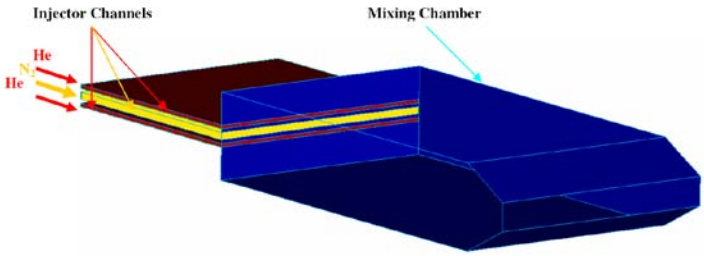

Figure 1: Three-Dimensional view of mixing chamber together with injector channels.

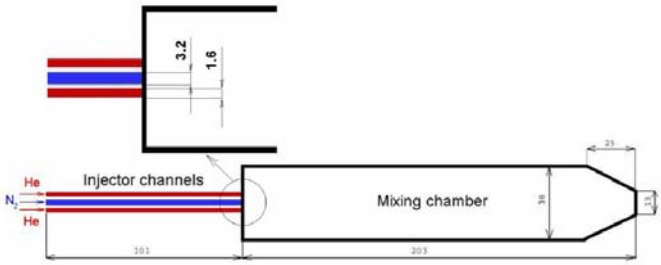

Figure 2: Cross-sectional view of inlet channels and mixing chamber.

The experiments [14,15] started with the chamber filled with quiescent air at ambient pressure and were initiated by opening a fast-acting valve for the nitrogen stream while the helium valves remained closed. The duration of this 'nitrogen-only' flow was set at 500 *ms* as a conservative estimate of the requisite time for establishing quasi-steady nitrogen flow through the central channel and the mixing chamber. Following this, the helium valve was opened and helium was injected through the two outer injector passages into this existing nitrogen flowfield. Upon opening the helium valves, the helium first filled a plenum and then purged the remaining gas (presumably air) in the helium passages before initiating a transient mixing process between the start-up flow of helium and the quasi-steady flow of nitrogen.

Quantitative measurements of the nitrogen concentration in the chamber were made by adding a trace amount of NO with the nitrogen and measuring its concentration as a function of time after the helium valve was opened by planar laser-induced fluorescence [15]. Upon activating the helium valve after the 0.5 *s* interval of background nitrogen (and NO) flow, the helium first filled the manifold and then propagated through the 101.6 *mm* passages before starting to appear in the chamber. The interval between the valve actuation signal and the time that helium started to enter the chamber was approximately 30 *ms*.

Repeated experiments showed that the jitter between helium valve actuation and the first appearance of helium in the chamber was nominally one *ms* [14]. A background reference image was taken 20 *ms* after the helium valve was opened to document the nitrogen-only (absence of helium) conditions in the chamber. Following this, images were taken at various intervals up to 90 *ms*.

The objective of the experiments and the simulations was to investigate the mixing characteristics between this transiently started helium flow with the existing nitrogen background flow and the rate at which they approach stationary conditions.

COMPUTATIONAL MODEL

The computations involved numerical solutions of the Navier-Stokes equations complemented by a single energy equation, three species equations and a two-equation, k-ω turbulence model [20]. The numerical integration of the coupled system was accomplished by a second-order upwind, finite-volume spatial time-marching procedure with three-point backward differencing for the temporal discretization [21, 22, 23]. The upwind system was incorporated by means of an approximate Riemann solver with special eigenvalue control to minimize artificial dissipation in various flow regimes. A dual-time method was used to eliminate approximate factorization errors in the implicit formulation. The thermodynamic and transport properties of the fluids were taken as functions of pressure and temperature. Pertinent flow conditions for the simulations were taken from the experiments and are given in Table 1.

TABLE I: Flow Conditions at Inlet Channels

Parameter	Value	Units
N_2 Flow Rate	59.6	(gm/s)
He Flow Rate (total)	18.0	(gm/s)
He Flow Rate (per slot)	9.0	(gm/s)
N_2 Exit Flow Velocity	185.0	(m/s)
N_2 Exit Mach Number	0.53	(−)
He Exit Flow Velocity	352.0	(m/s)
He Exit Mach Number	0.36	(−)
N_2 Reynolds Number	40,000	(−)
He Reynolds Number	4,000	(−)

Upstream boundary conditions for the simulations consisted of specifying the total pressure of helium and nitrogen at the upstream end of the injector passages along with their respective stagnation enthalpies. No-slip, adiabatic conditions were applied as wall boundary conditions. The exit boundary conditions were enforced by adding an external domain outside the chamber that extended from upstream of the exit plane to considerably downstream. Conditions at the upstream and downstream ends of this external domain were treated as 'far-field' boundaries through which flow could enter or leave depending on the local velocity. The upper and lower surfaces of the external domain were moved a considerable distance away and were treated as parallel, inviscid walls. The presence of this outer domain enabled either inflow or outflow at the nozzle exit plane along with flow curvature, pressure gradients and pressure levels above or below ambient at the exit.

Both 2-D and 3-D simulations were conducted. The 3-D grid contained 5,000,000 cells. The 2-D grid was obtained by extracting one plane from the 100 span-wise cells of the three dimensional grid and contained 50,000 cells in total. The purpose of this grid was to compare 2-D and 3-D solutions on grids of similar resolution and to compare both representations with experimental data. In all cases, the grid nearest the wall was placed at a $y+$ of approximately unity to enable integration of the velocity profiles to the wall.

FLOW INITIATION AND ESTABLISHED BACKGROUND

As in the experiments, the computations were started by first establishing a transient flow of nitrogen into which helium was introduced at a later time. As initial conditions, all three channels and the mixing chamber were filled with nitrogen at zero velocity and atmospheric pressure. Nitrogen flow was initiated by breaking a diaphragm at the upstream end allowing nitrogen to begin flowing through the central channel. To distinguish the entering nitrogen from that which filled the channels and chamber prior to flow initiation, two distinct species, 'old' nitrogen and 'new' nitrogen, were defined. These two types of nitrogen were identical in properties, but were distinguished computationally to differentiate the fluid that entered the computational domain during the simulation from that introduced with the initial condition. This artifice provides a quantitative determination of the time required to remove effects of the initial condition. The nitrogen flow was then monitored until the background flow reached a statistically stationary condition rather than running for an arbitrary time of 500 *ms* as was done in the experiments. During the nitrogen-only part of the simulation, the two outer channels were blocked at the upstream end but open downstream, allowing mass to enter or leave these channels as the pressure inside them adjusted with the mixing chamber.

The primary purpose of this first step is to start from a simple initial condition and to document the characteristic time for replacing the fluid in the recirculation region at the upstream end of the mixing chamber. Once a stationary background nitrogen flow was established, helium flow was initiated by breaking diaphragms at the upstream end of both outer slots. Of particular interest is an understanding of the rate of change of the concentration of helium in the recirculation regions adjacent to the upstream face and outer walls. This characteristic flow turnover time is of crucial importance for unsteady flow computations in which stationary flow conditions have been established in this recirculation region.

TWO-DIMENSIONAL SIMULATION RESULTS

As a first step for understanding the qualitative features of the flowfield, 2-D solutions were run and are given first. These results are then compared with experimental measurements taken on the central span-wise plane. The following section compares span wise variations obtained from the 3-D calculations with the measurements.

Snapshots of the instantaneous concentration distribution at seven different times in the nitrogen-only portion of the simulation are shown in Fig. 3 for the mixing chamber, omitting the inlet channels and the external domain. As can be seen, the initial nitrogen jet stays along the center line for the first 2 *ms*. There is a vortex on each side of the jet. After 3 *ms* the vortices became uneven and the incoming nitrogen jet starts to meander across the mixing channel while still retaining the behavior of a jet. Next, multiple vortices are developed and the jet is pushed toward the wall. Note that the recirculation regions at the upstream end of the chamber remain mostly composed of old nitrogen but, after 10 *ms*, have been strongly affected by the incoming fluid. As a reference, the nominal entry velocity of the nitrogen was 185 *m/s*, corresponding to a mean velocity through the chamber of 15 *m/s* and a nominal flow through time of 13 *ms*. Clearly, the flow replenishment time in these upstream corners is longer than the flow-through time. To evaluate the initial fluid depletion time, we show the contours of old nitrogen for later times, 30 and 40 *ms*, in Fig. 4. Note that the contour level was narrowed to [0, 0.1] to give a better indication of the residual old nitrogen inside the mixing chamber.

Figs. 3 and 4 surprisingly indicate that the initial old nitrogen in the upstream, including the fluid in the recirculation region is eliminated first while the downstream sections are evacuated last. Substantial fractions (>10%) of initial old nitrogen exist at 30 *ms* and it is not until after approximately 40 *ms* that helium can begin to be injected. Thus, the characteristic time to remove all the old nitrogen was 40 *ms*.

In addition to the time required to remove the initial fluid in the chamber, stationary conditions cannot be reached until the pressure perturbations introduced into the chamber by the initial conditions have also been eliminated. For this problem, pressure perturbations take a relatively short time to decay. Fig. 5 shows the volume averaged pressure inside the mixing chamber as a function of time during the first 40 *ms* of the simulation. The chamber pressure initially increases in response to the compression wave created as nitrogen flow starts to flow through the middle injector passage and then decreases slowly to a reasonably stationary value as the acoustic waves associated with start-up decay. Fig. 5 shows that the pressure transient takes approximately 20 *ms* to reach stationary conditions where the fluctuation level remains at about 2%. Previous work on flow initiation and transient processes for unsteady flow problems [24, 25] has shown that the approach to stationarity can be controlled by either pressure equilibration or by initial fluid removal times. Both must be monitored to ensure stationary conditions are reached. Clearly, the longer time should be chosen as the time to establish stationary conditions. For the present problem, the fluid removal time is considerably longer than the pressure equilibration time and the 40 *ms* identified above is taken as the time at which a stationary background flow has been established into which helium can be injected.

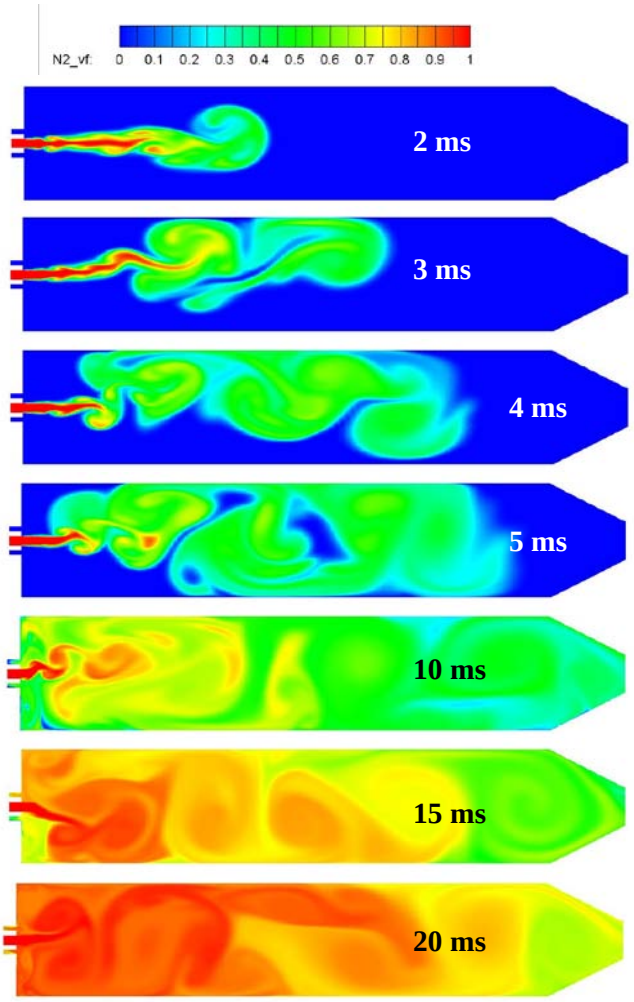

Figure 3: Instantaneous contours of New nitrogen injected into mixing chamber filled initially with Old nitrogen at time moments *t* = 2, 3, 4, 5, 10, 15, and 20 *ms*. (2-D).

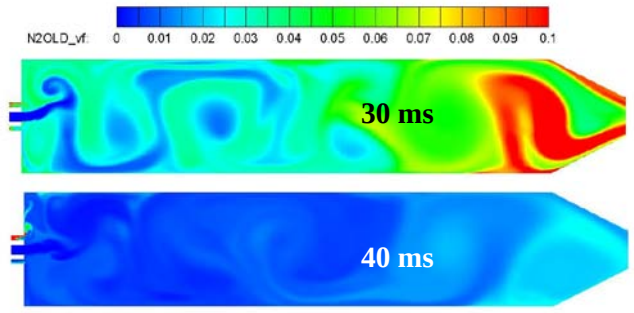

Figure 4: Instantaneous contours of Old nitrogen left inside the mixing chamber at time moments *t* = 30 and 40 *ms*.

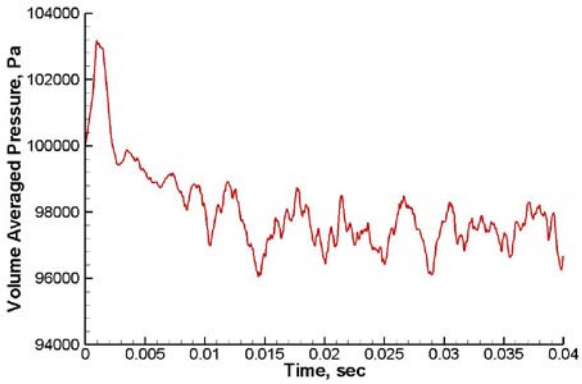

Figure 5: Time variation of chamber pressure from start of computation to beginning of stationary portion of solution.

TRANSIENT MIXING SOLUTIONS FOR HELIUM JET STARTUP INTO ESTABLISHED NITROGEN FLOW

The transient flow of helium was again controlled by specifying the stagnation pressure and temperature at the upstream end of both side channels. At the outset of the helium calculation, the fluid on the upstream side of the diaphragm was (quiescent) helium at the pressure and temperature corresponding to stagnation conditions. The fluid on the downstream side was trapped 'old' nitrogen at a pressure and temperature determined by instantaneous conditions in the mixing-chamber. The nitrogen inside the chamber at time t = 40 *ms* when the helium valve was opened to allow helium to enter through the upstream ends of the two outer channels exhibited a considerable amount of unsteadiness even though the stationary condition has been reached, as the Mach number contours in Fig. 6 show. The corresponding instantaneous contours of 'new' nitrogen at the time helium is turned on are shown in Fig. 7. Note that the greater portion of the helium channels contains trapped 'old' nitrogen, but that some new nitrogen has entered the downstream ends of the two outer injector channels. The distances it has penetrated into the channels, however, are not equal because of the asymmetric and unsteady behavior of the nitrogen (see Figs. 3 and 4). Consequently, helium begins to emerge from one injector channel sooner than from the other. This asymmetry in helium arrival time was also observed experimental results as shown later.

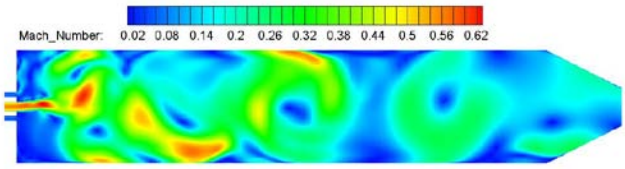

Figure 6: Snapshot of Mach number contours inside the mixing chamber at time moments t = 40 *ms*.

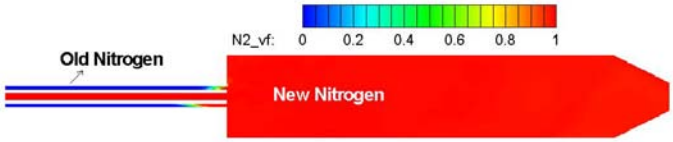

Figure 7: Snapshot of New nitrogen contours inside the injector and mixing chamber at time moments t = 40 *ms*.

The instantaneous helium concentration contours at different times are shown in Fig. 8. Helium first begins to enter the chamber at around 41.5 *ms*, 1.5 *ms* after helium flow initiation during the simulation. Because of the asymmetric structure of the background flow and the different amounts of nitrogen inside the helium injector channels, the helium enters from the upper channel slightly earlier than from the lower one. Small vortices develop near the injector exit and produce packets of helium that propagate downstream along the main nitrogen jet at earlier times. The leading portion of the helium mixes intensively with the background nitrogen flow causing the reattachment point to move upstream along the upper wall (compare with the nitrogen-only contours in Fig. 3). The oscillations in the near injector portion and the recirculation zones in the upper corner are clearly seen in the first four contours at time t = 41.5, 42, 42.5 and 43 *ms* in Fig. 8. Also note that the small vortex structures adjacent to the shear layer decay rapidly and the nitrogen-helium interface becomes smooth as the flow propagates downstream. This is due to the presence of lighter helium inside the chamber.

Another effect we can see from helium contours at time t = 43 and 43.5 *ms* in Fig. 8 is that the recirculation region at the upper side of the jet fills with helium faster than the one on the other side. Noting that the combined helium/nitrogen flow decreases the chamber flow-through time by approximately a factor of two (to approximately 7 *ms*), it is seen that the characteristic time in the recirculation zone is perhaps 10 times longer than the flow through time.

The helium jet reaches the nozzle entrance at approximately 45.5 *ms* and attaches to the bottom wall in the downstream portion of the chamber. By 47.5 *ms*, there is still a substantial amount of nitrogen left in the lower upstream corner where the helium finally fills after 49.5 *ms*. The entire chamber is filled with mixture with helium at a global mole fraction ratio of 40-50% at t = 57.5 *ms* as shown in the next to last plot in Fig. 8. After this, changes in the mixture are quite small over most of the chamber. Overall, the flowfield is highly dynamic and asymmetric with packets of helium rolling up and mixing with nitrogen inside the chamber.

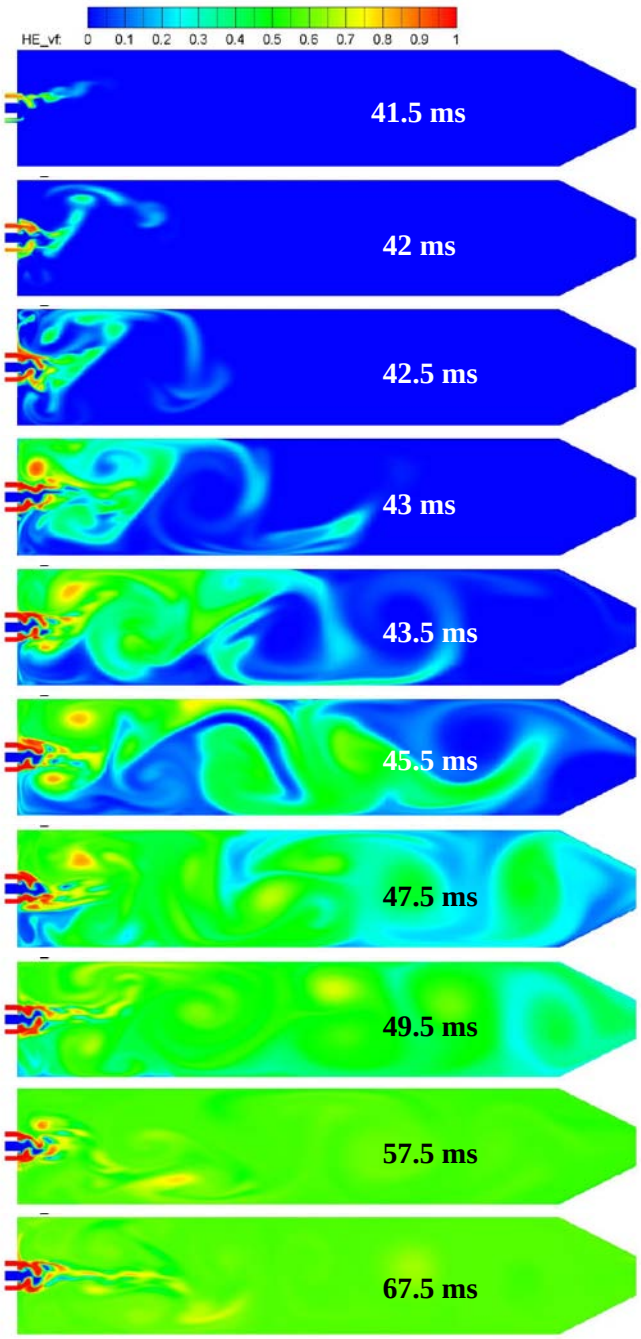

Figure 8: Sequence of time snapshots of mole fraction of helium injected into transient nitrogen background flow.

2-D COMPUTATIONAL/EXPERIMENTAL COMPARISON

Comparisons of results of the 2-D simulations with experimental results taken on the mid-plane of the chamber (where the 2-D approximation would appear to be most realistic) are shown in Fig. 9. This figure shows comparisons of the instantaneous helium concentrations in the computations with experimental results for four different time instants. The experimental PLIF images are on top and the numerical results are on the middle (2-D) and bottom (3-D). (Results from the 3-D calculation are discussed in the subsequent section.) To provide a meaningful comparison, the times have been adjusted so that the helium begins entering the chamber at the same time in both the experiment and the computation.

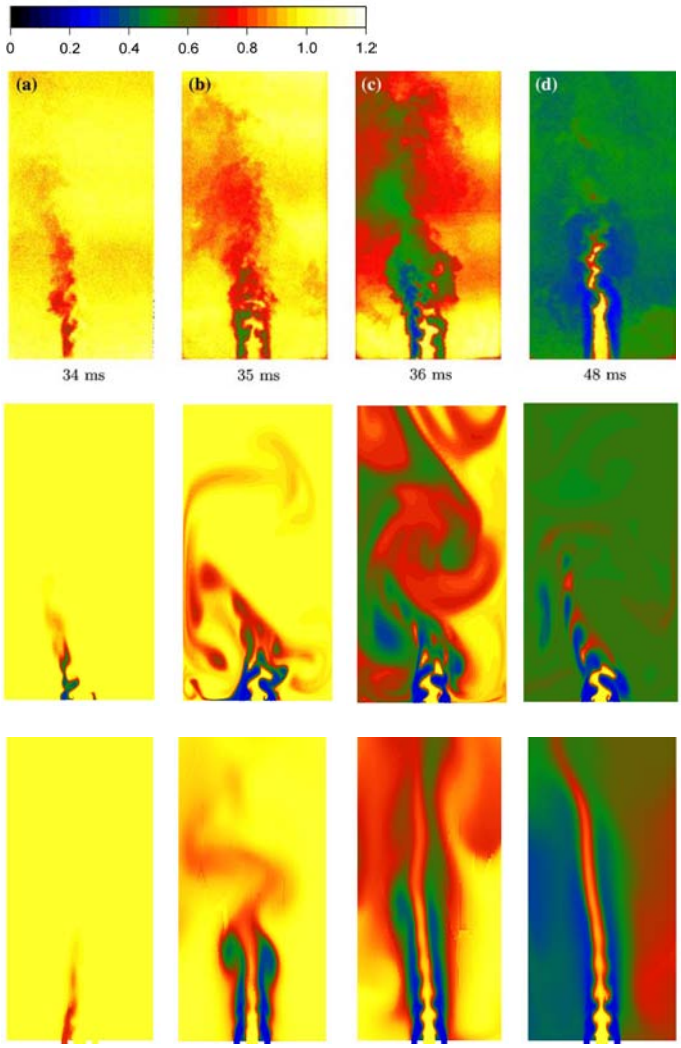

Figure 9: Nitrogen concentration contours at different times: a) *t* = 34 *ms*, b) *t* = 35 *ms*, c) *t* = 36 *ms*, d) *t* = 48 *ms*. Top: Experiment; Middle: 2-D Computation; Bottom: Mid-plane of 3-D computation.

The results in Fig. 9 show that the flow structure obtained in the 2-D computation is qualitatively similar to measured experimental conditions on the mid-span plane and the rates of development are similar. In both experiment and computation, the jet moves off center and both show a similar jet trajectory and width. The primary differences between the simulation and experiment are in the local details of the shear layer characteristics between the nitrogen and helium jets, though these are qualitatively correct.

To provide a more quantitative comparison of the spatial and temporal distribution of the nitrogen concentration, the time history of the helium mole fraction at four locations in the near field of the injector were monitored during the experiment. The

locations of the probes for these line plots are shown on Fig. 10. For convenience, the four locations are designated as the left and right bottom (LB and RB), and left and right top (LT and RT) positions. These designations are referenced to an injector that feeds the chamber from the face at the bottom to the nozzle at the top. The two 'bottom' probes were located 1mm from the injector face while the two 'top' probes were located 50 *mm* from the face. The 'left' and 'right' positions of the probes were located equally distant between the side walls and center line, 11.5 *mm* from the center plane. This same designation is also used for later results.

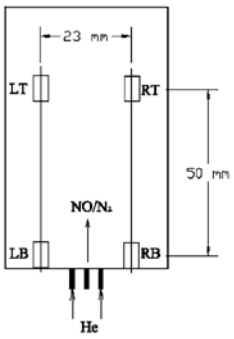

Figure 10: Schematic of locations referred for the baseline case in the first quarter of mixing chamber.

Experimental/computational comparisons of the time history of the mole fractions of nitrogen at the four referenced locations are shown in Fig. 11. The computational results are shown by the solid green lines while the experimental measurements are denoted by the red square symbols. The time, $t = 0$ is set at the time that the nitrogen valve was opened in the experiment (with the experimental times adjusted so that the first helium entered at the same time as in the computation). The complete duration of the simulation was 100 *ms*, of which the first 40 *ms* was the nitrogen-only injection and the helium valve was actuated at 40 *ms* in the computations.

The 40 *ms* transient time required to establish stationary background flow can be from the time history of the nitrogen concentrations at these four locations as well. The old nitrogen was replaced first at the LT location, followed by the RT location. This is consistent with the nitrogen contours shown in Fig. 3. At time 40 *ms*, the nitrogen concentrations reach the maximum value of unity for all locations, indicating new nitrogen has filled in the entire mixing chamber.

Fig. 11 shows that the nitrogen concentration decreases from 100% to about 40% during the first 10 *ms* in both computational results and experimental measurements. The nitrogen concentrations at these locations oscillate strongly reflecting the strong unsteady mixing inside the chamber. The figure also demonstrates that the transient time of the helium/nitrogen mixing process is about 20 *ms*, after which the nitrogen concentration reaches a stationary value for all four monitored locations. The transient process for the jet mixing on an established stationary background flow is about one-half the value required for establishing a stationary, nitrogen-only background flow.

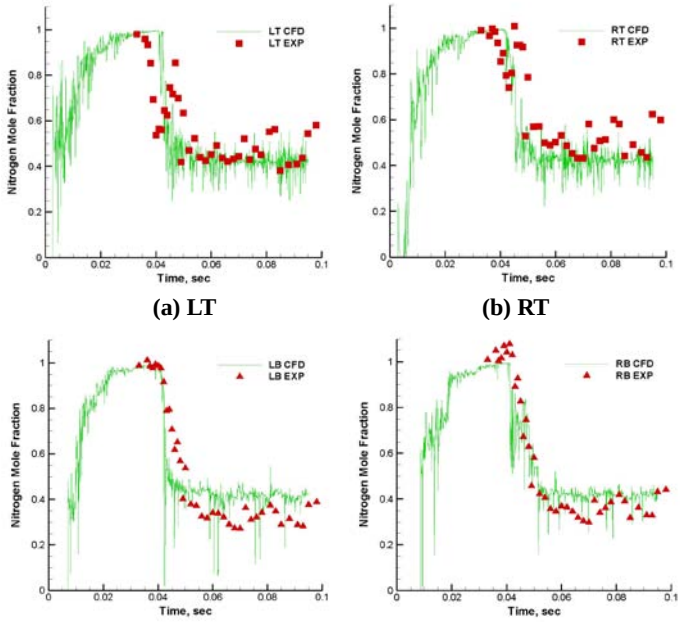

(a) LT **(b) RT**

(c) LB **(d) RB**

Figure 11: Comparison between experiments and computations of nitrogen mole fraction at four locations.

Overall, the flow structures and mixture distributions obtained in the numerical simulations are in good agreement with the mid-span experimental images and quantitative concentration measurements. The 2-D DES method is able to capture both the asymmetric and unsteady dynamics inside the mixing chamber in reasonable fashion. Certainly, the problem is three-dimensional but these 2-D results provide a background for 3-D calculations.

THREE-DIMENSIONAL SIMULATIONS

The 3-D simulations were done in the same manner as the 2-D calculations: a stationary background flow of nitrogen was first established followed by the introduction of helium. The goal of the 3-D calculations is to identify the manner in which 3-D solutions differ from the 2-D approximation.

As a first look at the 3-D solutions, we present a time series of new nitrogen mole fraction contours to evaluate the transient time required for the nitrogen-only injection to establish a stationary background flow. Fig. 12 shows of the mass fraction of new nitrogen along with iso-surfaces of new nitrogen at four different times, $t = 2$, 5, 10 and 20 *ms*. The contour plots shows five different span-wise planes, 2, 25, 50, 75 and 98% from one end wall. The iso-surface plots show surfaces of nitrogen mole fraction at concentration levels of 0.25, 0.5, 0.5 and 0.8 at the four times, respectively.

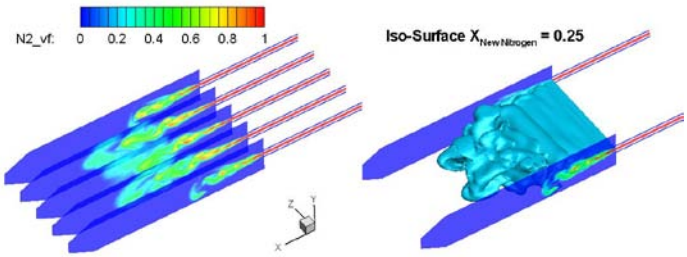

(a) t = 2 *ms*

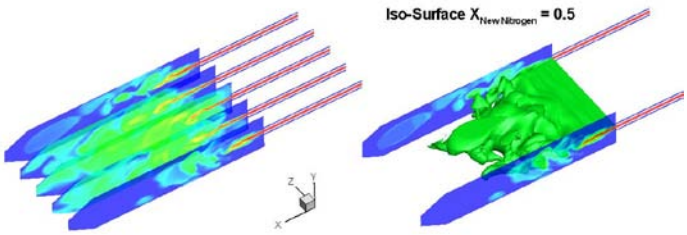

(b) t = 5 *ms*

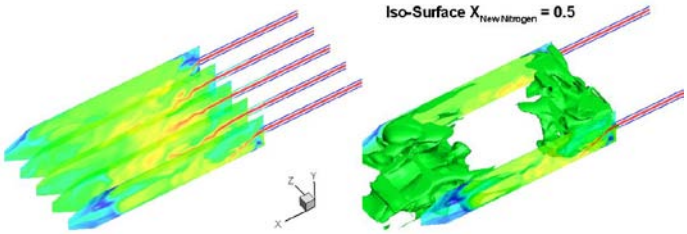

(c) t = 10 *ms*

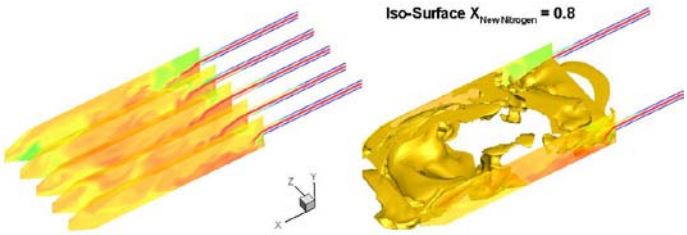

(d) t = 20 *ms*

Figure 12: Instantaneous contours and iso-surface of new nitrogen injected into mixing chamber at times, t = 2, 5, 10 and 20 *ms*.

While the results clearly show 3-D effects near the end walls, there remains much similarity with the 2-D results in the middle portion of the channel (compare Fig. 2). At the two earliest times, t = 2 and 5 *ms*, the central portion of the new nitrogen jet initially propagates downstream in the chamber, then begins to deviate from the center line and approach one side wall in very similar fashion to the 2-D solution. Strong 3-D effects are, however, observed near the end walls at the 2% and 98% span locations where the rate of penetration of the jet is substantially reduced by the nonslip boundary condition. The unsteady structures in the iso-surface plots also indicate significant 3-D effects near the center of the chamber. Overall, the nitrogen mole fraction contours are both smoother and more convoluted than the 2-D results, suggesting enhanced mixing due to the velocity and recirculation in the *x*-*z* and *y*-*z* planes.

The transient time required to deplete the initial old nitrogen in the chamber and establish a stationary 3-D background flow is also longer than in the 2-D case as can be seen by comparing the later time results in Fig. 13 with the 2-D results in Fig. 4. As in Fig. 4, the contour levels in Fig. 13 have also been narrowed to [0, 0.1] to give a better indication of the amount of residual old nitrogen inside the mixing chamber. At t = 30 *ms*, the mole fractions of old nitrogen are above 10% in most of the 3-D solution (Fig. 13a), while for 2-D solution, they are less than 10% inside the chamber except for a small region downstream near the nozzle (Fig. 4a). The 2-D results in Fig. 4 show that nearly all the old nitrogen has been removed by t = 40 *ms*, whereas the contour plots in Fig. 13 show large fractions of the 3-D have 5% of old nitrogen present at 40 *ms* and even at 60 *ms* the level of old nitrogen in the 3-D chamber are larger than those in the 2-D chamber at 40 *ms*. The apparent reason for this is the many more recirculation pockets in the 3-D solution which tend to prolong the depletion time.

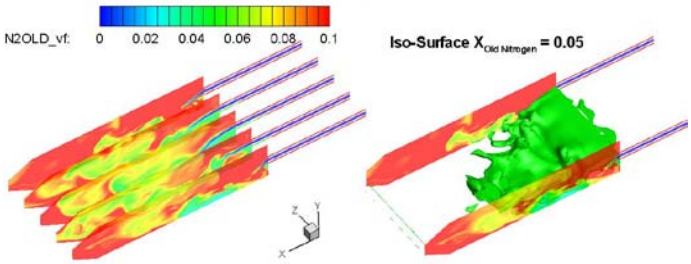

(a) t = 30 *ms*

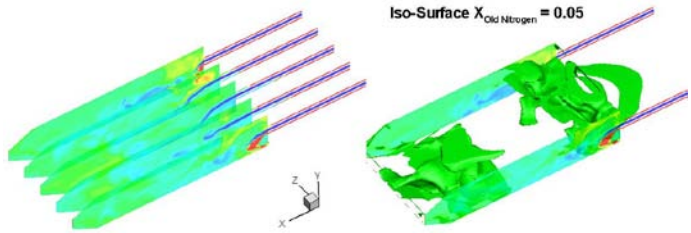

(b) t = 40 *ms*

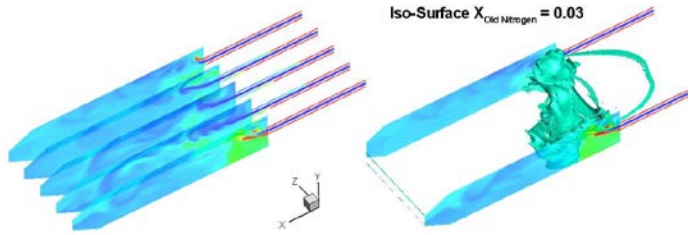

(c) t = 60 *ms*

Figure 13: Instantaneous contours and iso-surface of old nitrogen left inside the mixing chamber at different time moments. 3-D simulation.

The time variation of the volume averaged pressure for the 3-D simulation is plotted in Fig. 14. Comparing it with the one in Fig. 5, we find that the pressure transients take only about 5 *ms* to reach stationary level, which is much shorter than that required for the 2-D simulation. The 3-D results show a

pressure peak of similar magnitude at the beginning, but smaller pressure fluctuations inside the chamber following this. The 3-D geometry apparently has higher capabilities for damping pressure perturbations than the 2-D geometry.

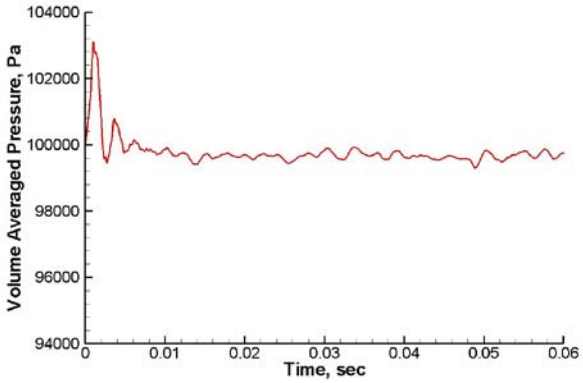

Figure 14: Time variation of chamber pressure from start of computation to beginning of stationary portion of solution. 3-D simulation.

Fig. 15 records the instantaneous helium mole fraction contours at different times in the 3-D simulation. Again, the global characteristics of the 3-D jet are similar to those observed in the 2-D simulations. Helium first begins to enter the chamber about 1.5 *ms* after the helium flow was initiated. As in the 2-D solution, the asymmetric structure of the background flow (Fig. 13c) causes the helium to enter the chamber at slightly times for the two channels. As the helium jet propagates through the chamber, it also deviates from the centerline and approaches one wall.

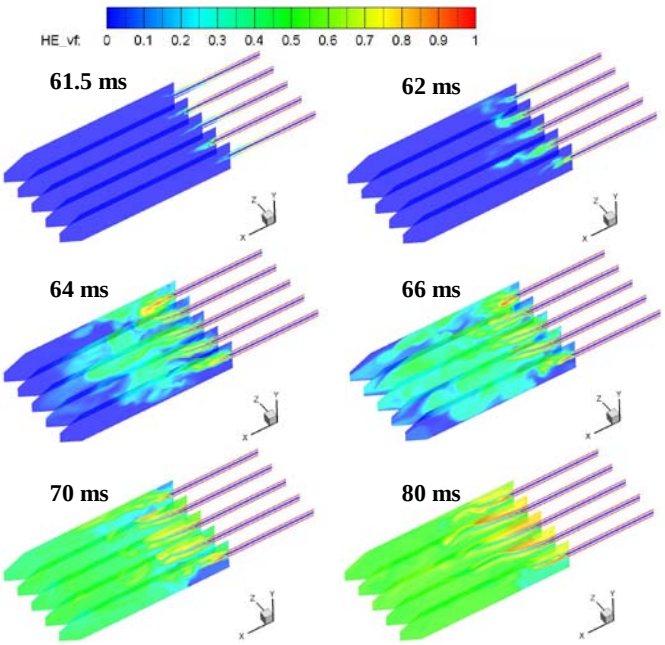

Figure 15: Sequence of time snapshots of mole fraction of helium injected into transient nitrogen background flow. 3-D simulation.

The helium structures exhibit a considerable amount of three dimensionality throughout the simulation. The attachment point on the wall is a strong function of span-wise position, and the large scale 3-D perturbations affect the dominant vortices in the entire flowfield. There are considerable span-wise variations inside the chamber. Comparing the mid-span (50%) helium mole fraction contours at later times with the 2-D results, it is seen that the 3-D nitrogen jet extends further and contains less unsteady structures. A relatively high concentration of helium appears in the upper corner of the chamber while in the 2-D results, the helium is more uniformly distributed throughout the chamber.

The nitrogen contours on the 50% span-wise plane of the 3-D calculation are compared with experiment and the 2-D results in Fig. 9. The numerical and experimental results both consistently show a deviation of the jet from the center line. Similar to the 2-D computational results, the initial exit of the two helium jets was slightly different times as seen in the figure on the left for t = 34 *ms*. At t = 35 *ms*, helium is flowing from both side channels and beginning to move toward the chamber wall. One millisecond later, the flow has moved further downstream and helium is now present at both walls. A saw-like structure is observed in the shear layer of the central nitrogen jet.

In the early time after the helium jet emerges into the chamber, both 2-D and 3-D simulations provide quantitatively similar results to the experimental PLIF images, while at 48 *ms*, the 3-D simulation over predicts the nitrogen concentration near the right side (Fig. 9d). In addition, the central nitrogen jet is too long as compared with experimental image. The 2-D simulation results seem to have better agreement with the experimental measurement than the 3-D results. We believe this is due to the relatively coarse grid near the 50% span-wise location in the 3-D simulation. The unsteady structures cannot be captured without enough grid resolution.

Next, we compare the simulation results with the PLIF images taken at two other span locations corresponding to 25% and 1% of the distance from the end wall. Corresponding numerical results are taken from four locations. The pair at 25% and 75% corresponds to the experiments at 25%, and the other pair at 1% and 99% corresponds to the 1% location in the experiment. The pairs of locations are shown because the configuration is symmetric in the span direction and comparing both locations provides more information especially when the flow is asymmetric. Since laser sheets could not be formed simultaneously in the experiments, simultaneous experimental results could not be obtained at both 1% and 99%.

The instantaneous results at time of 37 *ms* are compared in Fig. 16. The 3-D simulation results match the experimental measurements quite well at these two span-wise locations. (Note that the span-wise mesh size near the walls was very fine because the boundary layer was resolved within one wall unit, hence, the grid-induced deterioration seen at the mid-plane location is not present here.

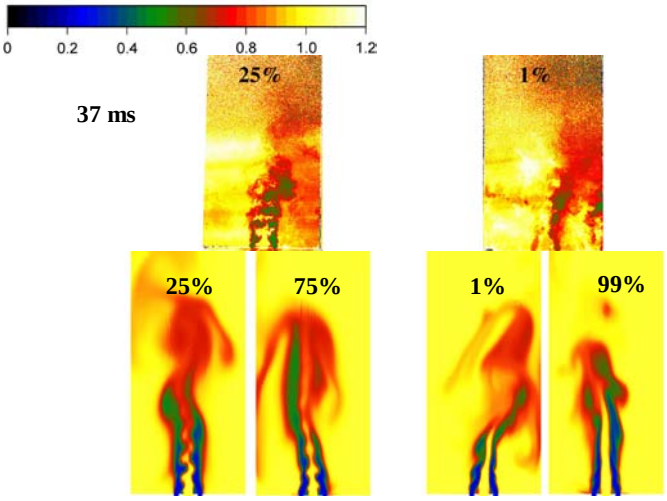

Figure 16: Comparisons of experiment (top) and computational Nitrogen concentration contours (bottom) at time moment *t* =37 *ms*. Computational results taken from 3-D simulation at four span locations.

As a final comparison with experiment, we show the spatial and temporal distribution of the nitrogen concentration at the four locations shown in Fig.10. Similar to the previous 2-D validations (Fig. 11), the 3-D computational results at 50% span location are compared with the experimental data in Fig. 17. The 3-D simulation captures the transient mixing process quite well at these four locations, however, it under predicts the nitrogen concentration at the left two locations. Comparing 2-D and 3-D, we find the 2-D simulation has better agreement with the experiment.

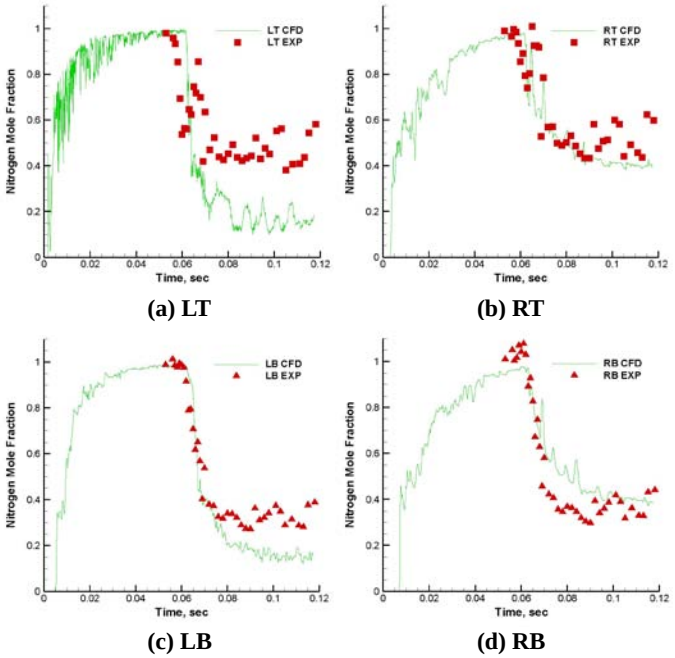

(a) LT **(b) RT**

(c) LB **(d) RB**

Figure 17: Comparison between experiments and computations of nitrogen mole fraction at four locations. Computational results taken from 3-D simulation at 50% span location.

SUMMARY AND CONCLUSIONS

Numerical simulations of the confined, transient mixing between gases of different molecular weights are presented. The geometrical configuration and flow conditions of interest are from a recent experiment. The gases were injected into a mixing chamber through three slots fed by long, narrow passages whose length was sufficient to ensure the incoming profiles were turbulent and fully developed. The mixture of gases exited the chamber through a short unchoked nozzle. Nitrogen was introduced through the central channel, and helium was injected through the side channels giving a fourteen to one density ratio. The objective of the study was to trace the evolution of the flow and mixing processes in the chamber. The mixing process was initiated by first establishing a background flow of nitrogen through the central channel and, upon reaching stationary conditions, starting the helium streams in a manner analogous to that used in the experiments. Both 2-D and 3-D simulations have been completed.

The starting process for the nitrogen-only background flow indicated a highly unsteady, asymmetric nitrogen stream in both the 2-D and 3-D simulations. In the middle of the chamber, the 3-D results were qualitatively similar to the 2-D calculation, but there were substantial 3-D effects near the end walls where the additional no-slip boundary condition dominated. The global results of this 3-D mixing indicated a transient time required for reaching stationary conditions in the 3-D simulation was approximately 50% longer than for the 2-D solution because of recirculation regions in the *x*-*z* and *y*-*z* planes.

After establishing the nitrogen background flow, helium was injected in both calculations. Both computational and experimental results indicate the flow remains asymmetric, is three-dimensional and is highly unsteady. The 2-D simulations give reasonable predictions on the chamber mid-plane but fail to predict the finite length effects that are encountered on the end walls. The 2-D predictions were in better agreement with the measurement, probably because the span-wise gird is highly stretched in the middle. The 3-D results agreed reasonably well with the measurements in the near-wall region where the span-wise grid was relatively fine. The experimental and the 2-D and 3-D computational results all indicated the two helium streams entered the chamber about a millisecond apart because of the asymmetric background flowfield. The initiation of the helium flow creates disruptions in the central nitrogen jet, but these disappear as the helium flow becomes established. Validation results show that the assumption of 2-D flow remains reasonable for the center plane, but 3-D analysis is required to match off-center-plane measurements.

ACKNOWLEDGMENTS

This project is supported by the NASA Constellation University Institutes Project (CUIP) program under Grant NCC8-200 with Ms. Claudia Meyer and Dr. Jeff Rybak of Glenn Research Center as contract monitors.

REFERENCES

1 Jahnke S, Kornev N, Tkatcheno I, Hassel E, Leder A (2005) Numerical study of influence of different parameters on mixing in a coaxial jet mixer using LES. Heat Mass Transfer 41:471- 481

2 Feng H, Olsen MG, Liu Y, Fox RO, Hill JC (2005) Investigation of turbulent mixing in a confined planar-jet reactor. AIChE J 51(10):2649-2664

3 Feng H, Olsen MG, Hill JC and Fox RO (2007) Simultaneous velocity and concentration field measurements of passive scalar in a confined rectangular jet. Exp Fluids 42:847-862

4 Stanley SA, Sarkar S, Mellado JP (2002) A study of the flowfield evolution and mixing in a planar turbulent jet using direct numerical simulation. J Fluid Mech 450:377-407

5 Johnson BV, Bennett JC (1981) Mass and momentum turbulent transport experiments with confined coaxial jets. NASA Contractor Rep. NASA, CR-165574, UTRC Rep R81-915540-9

6 Durst F, Pereira JFC and Tropea C (1993) the plane symmetric sudden-expansion flow at low Reynolds numbers. J. Fluid Mech 248:567-581

7 Fearn RM, Mullin T and Cliffe KA (1990) Nonlinear flow phenomena in a symmetric ducts with sudden expansion. J. Fluid Mech 211:595-608

8 De Zilwa SRN, Khezzar L, Whitelaw JH (2000) Flows through plane sudden-expansions J. Numer Meth Fluids 32:313-329

9 Balarac G, Si-Ameur M, Lesieur M, Metais O (2007) Direct numerical simulations of high velocity ratio coaxial jets: mixing properties and influence of upstream conditions. J. Turbulence 8(22):1-27

10 Tkatchenko I, Kornev N, Jahnke S, Steffen G and Hassel E (2007) Performance of LES and RANS models for simulation of complex flows in a coaxial jet mixer. Flow Turbulence and Combustion 78:111-127

11 Akselvoll K, Moin P (1996) Large-eddy simulation of turbulent confined coannular jets. J Fluid Mech 315:387-411

12 Baloch A, Townsend P and Webster MF (1995) On two- and three-dimensional expansion flows. J Comp & Fluids 24(8):863-882

13 Tseng CC, Kulatilaka WD and Lucht RP (2006) Laser imaging of transient mixing in a simulated chamber. AIAA Paper No. 2006-4530, July 2006

14 Tseng CC, Kulatilaka WD, Bhuiyan A, Merkle CL and Lucht RP (2007) Laser imaging of transient injection and mixing in a simulated rocket chamber. AIAA Paper No. 2007-5589, July 2007

15 Tseng CC, Voytovych DM, Kulatilaka WD, Bhuiyan AH, Lucht RP, Merkle CL, Hulka JR and Jones GW (2009) Structure and mixing of a transient flow of helium injected into an established flow of nitrogen: two dimensional measurement and simulation. Exp Fluids (2009) 46:559–575

16 Travin A, Shur M, Strelets M and Spalart PR (2000) Physical and Numerical Upgrades in the Detached-Eddy Simulation of Complex Turbulent Flows. In 412 EUROMECH Colloquium on LES of Complex Transitional and Turbulence Flows, Munich, Oct. 2000, Book of Abstracts

17 Menter FR and Egorov Y (2005) A Scale-Adaptive Simulation Model Using Two-Equation Models. AIAA Paper 2005-1095

18 Basu D, Hamed A and Das K (2005) DES, Hybrid RANS/LES and PANS Models for Unsteady Separated Turbulent Flow Simulations. FEDSM2005-77421, Proceedings of FEDSM'05

19 Baurle RA, Tam C-J, Edwards JR and Hassan HA (2003) Hybrid Simulation Approach for Cavity Flows: Blending, Algorithm, and Boundary Treatment Issues. AIAA J., Vol. 41, No. 8, pp. 1463-1480

20 Wilcox DC (1998) Turbulence modeling for CFD, 2nd Ed. DCW Industries, La Canada

21 Li D, Xia G, Merkle CL (2003) Analysis of real fluid flows in converging diverging nozzles. AIAA Paper 2003-4132

22 Li D, Sankaran V, Merkle CL, Lindau J (2005) A unified computational formulation for multi-component and multi-phase flows. AIAA Paper 2005-1391

23 Lian C, Xia G and Merkle CL (2009) Solution-Limited Time Stepping to Enhance Reliability in CFD Applications. Journal of Computational Physics, 228: 4836-4857

24 Lian C, Merkle CL and Xia G (2010) Flowfield Initialization and Approach to Stationary Conditions in Unsteady Combustion Simulations. Computers & Fluids, 39: 310-323

25 Lian C, Xia G and Merkle CL (2009) Effects of Back-Step Height and Recirculation Zones on Unsteady Mixing and Combustion. The 39th AIAA Fluid Dynamics Conference, June 22-25, 2009, San Antonio, TX